Published in final edited form as:
Biomaterials. 2011 May ; 32(13): 3435–3446. doi:10.1016/j.biomaterials.2011.01.021.

The effect of surface charge on *in vivo* biodistribution of PEG-oligocholic acid based micellar nanoparticles

Kai Xiao[a,e,1], **Yuanpei Li**[a,1], **Juntao Luo**[a,*], **Joyce S. Lee**[a,d], **Wenwu Xiao**[a], **Abby M. Gonik**[b], **Rinki Agarwal**[b], and **Kit S. Lam**[a,c,**]

[a]Department of Biochemistry & Molecular Medicine, UC Davis Cancer Center, University of California Davis, Sacramento, CA 95817, USA

[b]Division of Gynecologic Oncology, Department of Obstetrics and Gynecology, UCD Cancer Center, University of California Davis, Sacramento, CA 95817, USA

[c]Division of Hematology and Oncology, Department of Internal Medicine, University of California Davis, Sacramento, CA 95817, USA

[d]Department of Pharmacy, University of California, Davis Medical Center, Sacramento, CA 95817, USA

[e]National Chengdu Center for Safety Evaluation of Drugs, West China Hospital, Sichuan University, Chengdu 610041, China

Abstract

To systematically elucidate the effect of surface charge on the cellular uptake and *in vivo* fate of PEG-oligocholic acid based micellar nanoparticles (NPs), the distal PEG termini of monomeric PEG-oligocholic acid dendrimers (telodendrimers) are each derivatized with different number (n = 0, 1, 3 and 6) of anionic aspartic acids (negative charge) or cationic lysines (positive charge). Under aqueous condition, these telodendrimers self-assemble to form a series of micellar NPs with various surface charges, but with similar particle sizes. NPs with high surface charge, either positive or negative, were taken up more efficiently by RAW 264.7 murine macrophages after opsonization in fresh mouse serum. Mechanistic studies of cellular uptake of NPs indicated that several distinct endocytic pathways (e.g., clathrin-mediated endocytosis, caveolae-mediated endocytosis, and macropinocytosis) were involved in the cellular uptake process. After their cellular uptake, the majority of NPs were found to localize in the lysosome. Positively charged NPs exhibited dose-dependent hemolytic activities and cytotoxicities against RAW 264.7 cells proportional to the positive surface charge densities; whereas negatively charged NPs did not show obvious hemolytic and cytotoxic properties. *In vivo* biodistribution studies demonstrated that undesirable liver uptake was very high for highly positively or negatively charged NPs, which is likely due to active phagocytosis by macrophages (Kupffer cells) in the liver. In contrast, liver uptake was very low but tumor uptake was very high when the surface charge of NPs was slightly negative. Based on these studies, we can conclude that slightly negative charge may be introduced

*Corresponding author. Tel.: +1 916 734 0905; fax: +1 916 734 6415, juntao.luo@ucdmc.ucdavis.edu (J. Luo).. **Corresponding author. Tel.: +1 916 734 0910; fax: +1 916 734 4418, kit.lam@ucdmc.ucdavis.edu (K. S. Lam)..
[1]Kai and Yuanpei contributed equally to this work.
iamxiaokai@hotmail.com (K. Xiao)

to the NPs surface to reduce the undesirable clearance by the reticuloendothelial system (RES) such as liver, improve the blood compatibility, thus deliver the anti-cancer drugs more efficiently to the tumor sites.

Keywords

surface charge; nanoparticles; cellular uptake; macrophage; biodistribution; drug delivery

1. Introduction

Different types of nanoparticles (NPs), including liposomes, polymeric NPs, micellar NPs, albumin-based particles, inorganic or other solid particles (gold, iron oxide, quantum dots and carbon nanotubes) have been widely used as drug delivery vehicles for the diagnosis and targeted therapy of cancers. Early clinical results suggest that some nanoparticle therapeutics can enhance the therapeutic efficacy of delivered drugs while reducing their side effects, which can be explained by the preferential delivery of loaded drugs to tumor sites via the enhanced permeability and retention (EPR) effect [1]. The physicochemical characteristics of NPs such as composition, particle size, surface charge and surface hydrophobicity may affect their interaction with plasma proteins (opsonins) and blood components (hematocompatibility), uptake and clearance by macrophages, and hence potentially influence their biodistribution and targeted delivery of payload to the intended target sites [2]. The desired particle size of NPs for passive tumor targeting has been reported to be around 10–100 nm [3]. Hydrophilic polymers such as polyethylene glycol (PEG) have been widely used to coat the surface of NPs, in order to minimize the rapid opsonization and subsequent sequestration of NPs by macrophages in the reticuloendothelial system (RES). PEG surface coating can counteract the hydrophobic and electrostatic interactions between NPs and plasma proteins or macrophages, resulting in less RES uptake and prolonged blood circulation time [4–6]. Surface charge is usually introduced onto certain types of NPs (such as iron oxide and gold) to improve stability and prevent from further aggregation in aqueous solution via the electrostatic repulsion [7,8]. It has been reported that surface charge is a very important factor to determine the efficiency and mechanism of cellular uptake, and the *in vivo* fate of NPs [6,9–12]. However, the optimum surface charges (e.g. positive, neutral or negative) and charge densities were reported differently for different nanoparticle systems, in order to prolong the blood circulation time, minimize the nonspecific clearance of NPs and prevent their loss to undesired locations. For example, Juliano et al. [10] reported that neutral and positively charged liposomes were cleared less rapidly than negatively charged ones, which could be explained by the tendency of negatively charged liposomes to coalesce in the presence of proteins and calcium ion in blood plasma. Conversely, Yamamoto et al. [13] demonstrated that both neutral and negatively charged PEG-PDLLA micelles exhibited no remarkable difference in their blood clearance kinetics; however, negatively charged micelles significantly reduced the non-specific uptake by liver and spleen, compared with neutral micelles, which was attributed to the electrostatic repulsion between negatively charged micelles and cellular surface. The inconsistent results from the above studies may be due to the difference of nanoparticle types, variation in stability of NPs resulted from surface charge, the nature of charged groups, and other confounding factors such as inhomogeneous particle sizes.

He et al. systematically studied the effects of particle size and surface charge on cellular uptake and biodistribution of chitosan derivative polymeric NPs [11]. However, the NPs applied in this study had large particle sizes (150 to 500 nm), which led to significant high liver uptake regardless the surface charges. We have recently developed a novel micellar nanocarrier with desired narrow-dispersed particle sizes of 20–60 nm for effective tumor

targeting drug delivery with minimum liver uptake [14–16]. These NPs are formed by the self-assembly of novel linear-dendritic block copolymers (named as telodendrimer) with engineerable and well defined structures, comprising polyethylene glycol (PEG) and dendritic cholic acids (CA). PEG^{5k}-CA_8 is a representative telodendrimer with optimal properties, where "5k" represents the molecular weight of PEG (5000 dalton) and "8" indicates the number of CA subunits in the telodendrimer. PEG^{5k}-CA_8 micelles exhibited high drug loading capacity, outstanding stability, preferential tumor accumulation via EPR effects, and superior anti-tumor effects when loaded with paclitaxel (PTX) in the human ovarian cancer (SKOV-3) xenograft mouse model [14].

To optimize our nanocarriers for efficient *in vivo* cancer drug delivery, we systematically studied the effects of particle surface charges on their *in vitro* cellular uptake by macrophages, cytotoxic effects, hemolytic properties and *in vivo* biodistribution in xenograft models. Different number (n = 0, 1, 3 and 6) of anionic D-aspartic acids (d) or cationic D-lysines (k) were conjugated onto the distal end of PEG chain in PEG^{5k}-CA_8 telodendrimer (the micellar subunit) to modulate the surface charge of the micellar NPs. This allowed us to systematically evaluate the effect of surface charge on the cellular uptake and *in vivo* biodistribution of NPs under the identical conditions, e.g. the same composition and similar particle sizes. The particle sizes and surface charges (zeta potential) of aspartic acids or lysines derivatized NPs were characterized by transmission electron microscopy (TEM) and dynamic light scattering (DLS), respectively. The uptake efficiencies, pathways and intracellular fates of different charged PEG^{5k}-CA_8 NPs were examined in RAW 264.7 murine macrophages. The hemolytic properties and *in vitro* cytotoxicities against RAW 264.7 cells of these nanoparticle preparations were also evaluated. Finally, the *in vivo* biodistribution and tumor targeting efficiency of different charged PEG^{5k}-CA_8 NPs after intravenous administration were investigated in nude mice bearing SKOV-3 human ovarian cancer xenograft via NIRF optical imaging.

2. Methods

2.1 Materials

Diamino polyethylene glycol (Boc-NH-PEG-NH_2, MW = 5000 Da) was purchased from Rapp Polymere (*Tübingen*, Germany). Fmoc-D-Asp(Otbu)-OH, Fmoc-D-Lys(Boc)-OH, and Fmoc-Lys(Fmoc)-OH were purchased from Anaspec, Inc. Hydrophobic NIRF dye DiD (1,10-dioctadecyl-3,3,30,30-tetramethylindodicarbocyanine perchlorate, D-307), 4', 6-diamidino-2-phenylindole (DAPI) and LysoTracker® Green DND-2 were purchased from Invitrogen. Paclitaxel (PTX) was purchased from AK Scientific Inc. (Mountain View, CA). Cholic acid, MTT [3-(4,5-dimethyldiazol-2-yl)-2,5 diphenyl tetrazolium bromide], endocytosis inhibitors including chlorpromazine hydrochloride, amiloride hydrochloride hydrate, filipin III and all other chemicals were purchased from Sigma-Aldrich.

2.2 Synthesis of aspartic acids or lysines derivatized PEG^{5k}-CA_8telodendrimers

Boc-NH-PEG^{5k}-CA_8 telodendrimer was first synthesized using Boc-NH-PEG-NH_2 (MW, 5000 Da), lysine and cholic acid as building blocks via solution phase condensation reactions as described previously [14]. Briefly, Fmoc peptide chemistry was used to couple Fmoc-Lys(Fmoc)-OH onto the unprotected amino group of PEG for three rounds to generate a third generation of dendritic polylysine. Cholic acid NHS ester was coupled to the terminal end of dendritic polylysine, resulting in Boc-NH-PEG^{5k}-CA_8 telodendrimer. Then, the Boc group on the PEG chain of the telodendrimer was deprotected with 50% (v/v) trifluoroacetic acid (TFA) in dichloromethane (DCM), and different number (n = 0, 1, 3 and 6) of Fmoc-D-Asp(Otbu)-OH (d) or Fmoc-D-Lys(Boc)-OH (k) were subsequently conjugated to the distal end of PEG chain of PEG^{5k}-CA_8 telodendrimer by using Fmoc peptide chemistry. The

primary amine at the N terminal of corresponding aspartic acids or lysines conjugated PEG^{5k}-CA_8 telodendrimer was acetylated by acetic anhydride. Finally, the Otbu groups of aspartic acids and Boc groups of lysines were removed to generate PEG^{5k}-CA_8 telodendrimer with different number of free carboxylic acids and primary amines, respectively. The telodendrimers were precipitated and washed three times with cold ether, dialyzed against water for 24 h and then lyophilized.

2.3 Preparation and characterization of aspartic acids or lysines derivatized PEG^{5k}-CA_8 NPs

Different number (n = 0, 1, 3 and 6) of D-aspartic acids (d) or D-lysines (k) derivatized PEG^{5k}-CA_8 telodendrimer was used to prepare the corresponding micellar NPs with various surface charge densities. The dry-down (evaporation) method was utilized as described previously [17]. Briefly, 10 mg telodendrimer were first dissolved in chloroform, mixed, and evaporated in rotavapor to obtain a homogeneous dry polymer film. The film was reconstituted in 1 mL phosphate buffered solution (PBS), followed by sonication for 30 min, allowing the polymer to self-assemble into micelles. Finally, the micelle formulation was filtered with 0.22 μm filter to sterilize the sample. The morphology of aspartic acids or lysines derivatized PEG^{5k}-CA_8 micellar NPs was observed by TEM. The particle size distribution and zeta potential of these NPs were measured by DLS using Zetatrac (Microtrac). The stability of these NPs was evaluated by monitoring the particle size of NPs in 50% fetal bovine serum (FBS) over time.

Hydrophobic near-infrared fluorescence (NIRF) dye DiD as drug surrogate was physically encapsulated in the core of micellar NPs, in order to track the *in vitro* cellular uptake and and *in vivo* biodistribution of these NPs. Briefly, 10 mg aspartic acids or lysines derivatized PEG^{5k}-CA_8 telodendrimer was dissolved in chloroform, along with 0.2 mg DiD dye and 1 mg paclitaxel (PTX). Then, the same procedure of blank micellar NPs preparation described above was followed. The fluorescence spectrum and intensities of DiD labeled NPs with different surface derivations were characterized by fluorescence spectrometry (SpectraMax M2, Molecular Devices, USA). The *in vitro* release profiles of DiD dye from NPs were measured by the dialysis method. Briefly, DiD loaded NPs with different surface derivations were injected into a 500 μL dialysis cartridge (MWCO, 3.5 KDa, Thermo Scientific, Rochford, IL). The cartridges were dialyzed against 500 mL 10 mg/mL bovine serum albumin (BSA) solution in the presence of activated charcoal at 37 °C at the rotation rate of 100 rpm. The fluorescence intensities of DiD dye remaining in the dialysis cartridge at different time points were measured by the fluorescence spectrometer.

The surface charge properties of aspartic acids or lysines derivatized PEG^{5k}-CA_8 NPs were further characterized by the agarose gel electrophoresis. 15 μL DiD labeled PEG^{5k}-CA_8 NPs displaying aspartic acids or lysines were loaded in 1% agarose gel and subjected to electrophoresis in the running buffer (pH 7.4) at 120 voltages for 30 min. The DiD fluorescently labeled NPs in the agarose gel were then imaged using Kodak imaging station 2000MM with the excitation at 625 nm and the emission at 700 nm.

2.4 Cell culture

RAW 264.7 murine macrophage cell line and SKOV-3 human ovarian adenocarcinoma cell line were purchased from American Type Culture Collection (ATCC; Manassas,VA, USA). RAW 264.7 cells and SKOV-3 cells were respectively cultured in Dulbecco's Modified Eagle's Medium (DMEM) and McCoy's 5a Medium supplemented with 10% fetal bovine serum, 100 U/mL penicillin G, and 100 μg/mL streptomycin at 37 °C using a humidified 5% CO_2 incubator.

2.5 Cellular uptake of different charged PEG^{5k}-CA$_8$ NPs

2.5.1 Cellular uptake by murine macrophages and human cancer cells

2.5.1.1 Confocal fluorescence microscopy: RAW 264.7 murine macrophages or SKOV-3 human ovarian cancer cells were seeded in 8-well chamber tissue culture slides (*BD* Biosciences, Bedford, MA, USA). When the cells were almost 80% confluent, DiD fluorescently labeled PEG^{5k}-CA$_8$ NPs with various surface charges were added into the serum-free medium, respectively. The chamber slides were incubated for 2 h in a 5% CO_2 incubator at 37 °C, then washed three times with cold PBS and fixed with 4% paraformaldehyde for 10 min. The nuclei were counterstained by DAPI. The slides were mounted with coverslips and observed by Olympus FV1000 laser scanning confocal fluorescence microscopy.

2.5.1.2 Flow cytometry: The quantitative cellular uptake of different charged NPs in RAW 264.7 macrophages or SKOV-3 tumor cells were measured by flow cytometry. Briefly, 3×10^5 RAW 264.7 cells or SKOV-3 cells were incubated with DiD labeled PEG^{5k}-CA$_8$ NPs with various surface charges in the serum-free medium for 30 min or 2 h. Then the cells were washed with PBS three times and resuspended in PBS for flow cytometry analysis (Stratedigm S 1400). 10, 000 events were collected for each sample.

2.5.1.3 The effect of opsonization in serum on the phagocytosis of different charged NPs: To investigate whether the opsonization of NPs in serum can affect their macrophage uptake, DiD labeled PEG^{5k}-CA$_8$ NPs with various surface charges were first incubated with either fresh or heat-inactivated mouse serum prior to being exposed to the RAW 264.7 cells. Heating the serum at 56 °C for 30 min can lead to the inactivation of the complement components. A total of 20 μL of the NPs suspension (10 mg/mL) were incubated with 100 μL of fresh or inactivated serum at 37 °C under constant shaking for 30 min. The pre-opsonized NPs were then incubated with RAW 264.7 cells for 2 h at 37 °C. The cells were subsequently washed with PBS three times, scraped, and resuspended in PBS for flow cytometry analysis.

2.5.2 Co-localization studies with lysosomes in live cells—RAW 264.7 cells were seeded in the coverglass chamber slides (VWR LabShop, Batavia, IL). After reaching 80% confluence, the cells were treated with DiD fluorescently labeled PEG^{5k}-CA$_8$ NPs with various surface charges. After 1.5 h, LysoTracker Green (50 nM) was added in the medium and the cells were incubated for another 30 min. The cells were rapidly washed with ice cold PBS to prevent the removal of the attached LysoTracker Green, and replaced with fresh medium, then the live cells were observed under the Olympus FV1000 laser scanning confocal fluorescence microscopy.

2.5.3 The uptake pathways of different charged NPs—The effect of temperature block was studied by pre-incubating the RAW 264.7 cells at 4 °C for 3 h and treatment with DiD fluorescently labeled PEG^{5k}-CA$_8$ NPs with various surface charges for 2 h at 4 °C. To study the effects of different endocytosis inhibitors on the cellular uptake of NPs, RAW 264.7 cells were pre-incubated for 1 h at 37 °C with the following inhibitors at concentrations that were not toxic to the cells: chlorpromazine (CPZ, 10 μg/mL) to inhibit the formation of clathrin vesicles, filipin III (1 μg/mL) to inhibit caveolae, or amiloride (50 μM) to inhibit macropinocytosis. Following the pre-incubation, DiD labeled PEG^{5k}-CA$_8$ NPs with various surface charges were added into the medium containing the inhibitors and the cells were incubated at 37 °C for 2 h. The cells were washed three times with ice cold PBS, fixed with fresh 4% paraformaldehyde for 10 min at room temperature, and the nuclei were stained with DAPI. The cells were visualized under the Olympus FV1000 laser

scanning confocal fluorescence microscopy. For quantitative analysis, the fluorescence intensities of the cells treated as above were also measured by flow cytometry.

2.6 Hemolysis

Fresh citrated blood was obtained from healthy human volunteers. First, 2 mL of blood was added into 10 mL of PBS, and then red blood cells (RBCs) were separated from plasma by centrifugation at 1000 × g for 10 min. The RBCs were washed three times with 10 mL of PBS solution, and resuspended in 20 mL PBS. Two hundred microliters of diluted RBC suspension was mixed with blank PEG^{5k}-CA_8 NPs with various surface charges at serial concentrations (20, 100 and 1000 μg/mL) by gentle vortex and incubated at 37 °C. After 4 h, the mixtures were centrifuged at 1000 × g for 5 min, and 100 μL of supernatant of all samples were transferred to a 96-well plate. Free hemoglobin in the supernatant was measured by the absorbance at 540 nm using a microplate reader (SpectraMax M2, Molecular Devices, USA). RBCs incubation with Triton-100 (2%) and PBS were used as the positive and negative controls, respectively. The percent hemolysis of RBCs was calculated using the following formula: RBCs hemolysis = $(OD_{sample} - OD_{negative\ control})/(OD_{positive\ control} - OD_{negative\ control}) \times 100\%$.

2.7 In vitro cell viability

The MTT assay was used to evaluate the effect of surface charge on the cell viability of PEG^{5k}-CA_8 NPs against RAW 264.7 macrophages [18]. Briefly, Raw 264.7 cells in 150 μL culture medium were seeded in 96-well plates at a density of 4×10^3 cells/well. After overnight incubation at 37 °C, different charged PEG^{5k}-CA_8 NPs in a volume of 50 μL were added to each well, respectively. After 72 h incubation in a humidified 37 °C, 5% CO_2 incubator, MTT was added to each well and further incubated for another 4 h. The absorbance at 570 nm and 660 nm was detected using the microplate ELISA reader. Untreated cells served as a control. Results were shown as the average cell viability $[(OD_{treat} - OD_{blank})/(OD_{control} - OD_{blank}) \times 100\%]$ of triplicate wells

2.8 In vivo biodistribution of different charged PEG^{5k}-CA_8 NPs

The *in vivo* biodistribution and tumor accumulation of different charged PEG^{5k}-CA_8 NPs were investigated in nude mice bearing SKOV-3 human ovarian cancer xenograft by the NIRF optical imaging approach. Female athymic nude mice (Nu/Nu strain), 7~8 weeks age, were purchased from Harlan (Livermore, CA). All animals were kept under pathogen-free conditions according to AAALAC guidelines and were allowed to acclimatize for at least 4 days prior to experiments. All animal experiments were performed in compliance with institutional guidelines and according to protocol No. 07-13119 approved by the Animal Use and Care Administrative Advisory Committee at the University of California, Davis. A subcutaneous ovarian cancer xenograft model was established by injecting 7×10^6 SKOV-3 cells in a 100 μL of mixture of PBS and Matrigel (1:1 v/v) subcutaneously at the right flank in female nude mice. Mice with subcutaneous SKOV-3 tumors of an approximate 8~10 mm diameter were subjected to *in vivo* imaging. DiD fluorescently labeled PEG^{5k}-CA_8 NPs with various surface charges in 100 μL PBS were injected intravenously into the tumor bearing mice via the tail vein, respectively (n = 3). At different time points (1 h, 2 h, 4 h, 8 h and 24 h) post injection, mice were scanned using a Kodak multimodal imaging system IS2000MM with an excitation bandpass filter at 625 nm and an emission at 700 nm. The mice were anaesthetized by intraperitoneal injection of pentobarbital (60 mg/kg) before each imaging. All animals were euthanized by CO_2 overdose at 24 h after injection. Tumors and major organs were excised and imaged with the Kodak imaging station. The fluorescence intensities were determined by the Kodak imaging station software using operator-defined regions of interest (ROI) measurements on tumors and other organs.

For the microscopic analysis, excised tumors and livers were frozen in O.C.T. (cryo-embedding medium) at 80 °C. The corresponding slices (10 μm) were then prepared with a Zeiss Microm HM500 microtome cryostat (Zeiss, Walldorf, Germany), air-dried for 30 min and fixed with 4% paraformaldehyde for 10 min. The macrophages (Kupffer cells) in the liver were stained by F4/80 rat anti-mouse primary antibody (1:200, AbD Serotec, Raleigh, NC) for 45 min, washed with PBS three times, then stained by Cy3 conjugated goat anti-rat IgG secondary antibody (1:500, Santa Cruz Biotechnology, Santa Cruz, CA) for 45 min. The nuclei were stained with DAPI, and the slides were mounted with coverslips and visualized with an Olympus FV1000 laser scanning confocal fluorescence microscopy.

2.9 Statistical analysis

The level of significance in all statistical analyses was set at a probability of $P < 0.05$. Data are presented as means ± standard error (SEM). Statistical analysis was performed by Student's t-test for comparison of two groups, and one-way analysis of variance (ANOVA) for multiple groups, followed by Newman-Keuls test if overall $P < 0.05$.

3. Results

3.1 Preparation and characterization of different charged PEG^{5k}-CA$_8$ NPs

To systematically modulate the surface charge density of PEG^{5k}-CA$_8$ NPs, different number (n = 0, 1, 3 and 6) of anionic D-aspartic acids (d, negative charge) or cationic D-lysines (k, positive charge) were chemically conjugated to the distal end of PEG strand constituting the shell layer of the micellar NPs, respectively (Fig. 1). After the conjugation of aspartic acids or lysines onto the PEG chain of PEG^{5k}-CA$_8$ telodendrimer, the N-terminal amino group was acetylated. The ^{1}H-NMR spectra of aspartic acids or lysines derivatized PEG^{5k}-CA$_8$ telodendimers have been collected in DMSO-d$_6$. As shown in Fig. S-1, the signals at 0.6–2.4 ppm and 3.5–3.7 ppm could be assigned to cholic acids and PEG chains, respectively. The peak at 2.8 ppm corresponds to the protons on the ε-methylene on the free lysine side chain, and this characteristic peak increases accordingly with the numbers of lysines in the telodendrimer (Fig. S-1A). However, the signals of aspartic acids are overlapped with the signals from the telodendrimers and no distinguishable signal was observed. (Fig. S-1B).

Seven kinds of PEG^{5k}-CA$_8$ NPs with various surface charge densities, including neutral acetylated NPs (Ac-NP), negatively charged NPs displaying single, triple and hexa aspartic acids (1d-NP, 3d-NP and 6d-NP) and positively charged NPs displaying the same number of lysines (1k-NP, 3k-NP and 6k-NP), were prepared, respectively. The morphology, particle size and surface charge of each nanoparticle preparation were subsequently characterized. Transmission electronic microscopy (TEM) images (Fig. 2) demonstrated that all PEG^{5k}-CA$_8$ NPs with different surface derivations were spherical, and their particle sizes were in the range of 15~20 nm in diameter, which was consistent with the results obtained from the DLS particle sizer (Fig. S-2). The zeta potential values (surface charges) of all nanoparticle preparations were measured by DLS Zetatrac, respectively. As expected, the zeta potential of PEG^{5k}-CA$_8$ NPs was dramatically influenced by the derivation with aspartic acids or lysines. The zeta potential of the Ac-NP was 3.6 ± 0.8 mV in deionized water. As the number of conjugated aspartic acids increased, the surface charge negativity of PEG^{5k}-CA$_8$ NPs increased accordingly, with the zeta potential of 1d-NP, 3d-NP and 6d-NP being −8.5 ± 1.8, −17.5 ± 0.9 and −26.9 ± 1.7 mV, respectively. Similarly, as the number of conjugated lysines increased, the surface charge positivity of PEG^{5k}-CA$_8$ NPs also increased, with the zeta potential of 1k-NP, 3k-NP and 6k-NP being 18.5 ± 3.1, 29.5 ± 1.2 and 37.0 ± 2.9 mV, respectively (Table 1). The non-proportional increase of the surface charge density with the increasing number of aspartic acids or lysines, can be explained by the decreased ionization

yield of the weak acids (−COOH) and weak bases ($-NH_2$) with the increased concentrations of the entities.

To track and "visualize" the cellular uptake and *in vivo* biodistribution of different charged PEG^{5k}-CA_8 NPs, all the NPs were rendered fluorescent via the encapsulation of a hydrophobic fluorescence probe DiD (0.2 mg/mL) along with chemotherapeutic drug PTX (1 mg/mL). There were no significant changes in the average particle sizes for all nanoparticle preparations after DiD/PTX loading, which were all in the range of 23 ~ 27 nm with the narrow size distribution. The emission spectra and fluorescence intensities of DiD labeled PEG^{5k}-CA_8 NPs with various surface charges were very similar, with the emission peak at 675 nm (Fig. S-3). To demonstrate the stability of the NPs in physiological conditions including blood, the prepared DiD fluorescently labeled NPs were incubated with 50% FBS for up to 72 h, and the particle sizes of NPs were monitored by DLS. There were no noticeable changes in the size distribution profiles for all the NPs with various surface charges (data not shown), which indicated that these NPs were able to maintain their stability during the *in vivo* application. The amount of DiD dye released from the NPs, after dialysis against 10 mg/mL bovine serum albumin (BSA) solution at 37 ℃, was found to be approximately 5% in 2 h, and <12% in 24 h (Fig. S-4). The surface charge properites of DiD labeled PEG^{5k}-CA_8 NPs with different surface derivations were further confirmed by agarose gel electrophoresis. As shown in Fig. 3, there was almost no mobility shift for Ac-NP after electrophoresis at 120 voltages for 30 min. However, PEG^{5k}-CA_8 NPs derivatized with aspartic acids or lysines migrated toward the expected positive electrode or negative electrode, respectively, and the migration distance increased with the increasing number of conjugated aspartic acids or lysines. In summary, we were able to prepare a series of PEG^{5k}-CA_8 NPs with precisely controlled surface charge, similar particle size and superior stability, which allowed us to subsequently investigate the effect of surface charge on the *in vitro* cellular uptake and *in vivo* biodistribution of the micellar NPs.

3.2 Cellular uptake of different charged PEG^{5k}-CA_8NPs by macrophages

DiD fluorescently labeled PEG^{5k}-CA_8 NPs with various surface charges were incubated with RAW 264.7 murine macrophages in the serum-free medium at 37 °C for 2 h. Internalization of fluorescently labeled NPs was visualized under a confocal fluorescence microscopy. As shown in Fig. 4, the red fluorescence coming from DiD labeled NPs was detected inside the cytosolic compartments of RAW 264.7 macrophages. The fluorescence intensity indicates the level of the internalization of NPs by the macrophages. It was clear that the surface charge played an important role in cellular uptake of PEG^{5k}-CA_8 NPs by the macrophages. In general, positively charged PEG^{5k}-CA_8 NPs were taken up more efficiently by macrophages, when compared with neutral or negatively charged PEG^{5k}-CA_8 NPs. The uptake efficiencies of PEG^{5k}-CA_8 NPs with various surface charges were further quantified by flow cytometry analysis. As illustrated in Fig. S-5A, all of the nanoparticle preparations were found to be taken up by RAW 264.7 macrophages in a time-dependent manner. Compared to neutral NPs, positive surface charges significantly increased the uptake efficiency of PEG^{5k}-CA_8 NPs ($P < 0.05$). After 2 h incubation with RAW 264.7 macrophages, the uptake efficiency of 1k-NP, 3k-NP, and 6k-NP were 1.9-fold, 3.5-fold and 5.9-fold of neutral Ac-NP, respectively. On the contrary, negative surface charges slightly decreased the uptake efficiency of PEG^{5k}-CA_8 NPs. In addition, the uptake profiles of different charged PEG^{5k}-CA_8 NPs were also investigated in SKOV-3 human ovarian cancer cells cultured in serum-free medium, and the results illustrated a charge-dependent uptake pattern of NPs very similar to that by macrophages (Fig. S-5 B).

It is known that the opsonization in the blood stream after systematic administration may affect the cellular uptake of NPs by macrophages [19]. To systematically study the effect of opsonization on the macrophage uptake of PEG^{5k}-CA_8 NPs, PEG^{5k}-CA_8 NPs with various

surface charges were pre-incubated with fresh mouse serum prior to cellular exposure. After opsonization, the macrophage uptakes of negatively charged NPs (6d-NP and 3d-NP) were significantly increased, compared to the non-opsonized ones ($P < 0.05$). However, opsonization resulted in slightly lower macrophage uptakes for the positively charged NPs (Fig. 5). Overall, PEG^{5k}-CA_8 NPs with slightly negative charge (1d-NP) had the lowest macrophage uptake in the presence of fresh mouse serum. Furthermore, the nature of serum employed was also found to have important effect on the uptake of NPs by macrophages. The phagocytic levels of all these NPs after opsonized in fresh mouse serum were higher than those after opsonized in heat-inactivated serum.

To track the intracellular fates of different charged PEG^{5k}-CA_8 NPs following their cell uptake, the lysosomal compartment of RAW 264.7 macrophages was stained with the Lysotracker Green probe [20], after the cells were incubated for 2 h with DiD fluorescently labeled NPs in medium that contained 10% fresh mouse serum. The Lysotracker Green, which is colorless at physiological pH, has green fluorescence at the acidic pH present in the lysosome. The co-localization of DiD labeled NPs (red) with lysosome (green) produced a yellow fluorescence in the merged images. As shown in the live-cell imaging (Fig. 6), the intracellular uptake of NPs in macrophages increased with the increasing surface charge densities (either positive or negative), and the majority of NPs were trapped inside the lysosome after their cellular uptake.

The pathways involved in the cellular uptake of different charged PEG^{5k}-CA_8 NPs were further explored (Fig. 7). First of all, the cellular uptake of NPs was found to be an active (energy-dependent) process, as evidenced by the significant reduction in the uptake of all the nanoparticle preparations at low temperature (4 °C) ($P < 0.05$). Next, several endocytosis inhibitors, each known to be specific against a particular endocytic pathway, were employed to determine the cellular uptake mechanisms of the NPs. As shown in the confocal microscopic images (Fig. 7A), all these endocytosis inhibitors were able to inhibit the macrophage uptake of different charged NPs to some extent, compared with the corresponding controls without the treatment of endocytosis inhibitors. The inhibition efficiencies of NPs uptake by those endocytosis inhibitors were further quantitatively measured by flow cytometry analysis. As shown in Fig. 7B, when RAW 264.7 macrophages were pre-incubated with filipin III, the cellular uptake of 6d-NP, 3d-NP, 1d-NP, Ac-NP, 1k-NP, 3k-NP, and 6k-NP were reduced by ca. 41%, 50%, 36%, 28%, 23%, 15% and 16%, respectively; Similarly, when cells were pre-incubated with amiloride, the cellular uptake of 6d-NP, 3d-NP, 1d-NP, Ac-NP, 1k-NP, 3k-NP, and 6k-NP were reduced by ca. 62%, 60%, 50%, 47%, 45%, 39% and 37%, respectively; More remarkably, when cells were pre-incubated with CPZ, the cellular uptake of 6d-NP, 3d-NP, 1d-NP, Ac-NP, 1k-NP, 3k-NP, and 6k-NP were reduced by ca. 85%, 80%, 79%, 75%, 65%, 61% and 55%, respectively. Taken together, the internalization of different charged PEG^{5k}-CA_8 NPs is mediated by the combinations of several cellular uptake mechanisms including clathrin-mediated and caveolae-mediated endocytosis as well as macropinocytosis.

3.3 Hemolysis study

The effect of surface charge on the hemolytic activity of blank PEG^{5k}-CA_8 NPs was evaluated by the hemolysis assay. Blank PEG^{5k}-CA_8 NPs with various surface charges, PBS (negative control) and 2% Triton-100 (positive control) were incubated with human RBCs suspension at 37 °C for 4 h, respectively. Lysis of RBCs was determined spectrophotometrically ($\lambda = 540$ nm) based on oxyhemoglobin level. As expected, there was no spontaneous RBCs lysis after incubation with PBS, and it was assumed that there was 100% RBCs lysis after incubation with Triton-100. Negatively charged NPs (1d-NP, 3d-NP, and 6d-NP) at the concentrations ranging from 20 μg/mL to 1 mg/mL had negligible hemolytic activities, whereas positively charged NPs (1k-NP, 3k-NP and 6k-NP) exhibited

dose-dependent hemolytic properties, and the hemolytic tendency significantly increased as the positive surface charge density increased ($P < 0.05$). For example, at the concentration of 1 mg/mL, the percentage of hemolysis induced by 1d-NP, 3d-NP and 6d-NP were 4.6%, 4.3% and 4.7%, respectively; however, that induced by Ac-NP, 1k-NP, 3k-NP and 6d-NP were 13.8%, 36.7%, 41.4% and 64%, respectively (Fig. 8).

3.4 In vitro cytotoxicity

The *in vitro* cytotoxicities of different charged PEG^{5k}-CA_8 NPs against RAW 264.7 macrophages were measured by MTT assay. At concentrations ranging from 0.4 mg/mL to 1 mg/mL, negatively charged NPs did not exhibit any observable toxic effects on the cell viability; in contrast, positively charged NPs did exert surface charge density-dependent cytotoxicities, with the more positive charged NPs the higher cytotoxic potential ($P < 0.05$). For example, at the concentration of 1 mg/mL, the average cell viability of RAW 264.7 cells after the treatment with 6d-NP, 3d-NP, 1d-NP, Ac-NP, 1k-NP, 3k-NP and 6k-NP was 102%, 114%, 109%, 96%, 85%, 73% and 41%, respectively (Fig. 9).

3.5 In vivo biodistribution of different charged PEG^{5k}-CA_8NPs

Noninvasive NIRF optical imaging approach was utilized to monitor the *in vivo* biodistribution and tumor accumulation of different charged PEG^{5k}-CA_8 NPs. The fluorescence labeling of NPs with NIRF dye DiD will ensure effective NPs tracking *in vivo*, as NIRF dyes enable deep tissue imaging with high penetration, low tissue absorption and scattering [21]. DiD-labeled PEG^{5k}-CA_8 NPs with various surface charges were injected via tail vein into the nude mice bearing SKOV-3 human ovarian cancer xenograft. The *in vivo* NIRF optical images demonstrated that all of different charged NPs were able to gradually accumulate at the tumor site starting at 2 h after administration, and the NPs were retained in the tumor throughout the 24 h period (Fig. S-6). However, NPs with neutral or slightly negative charge exhibited higher tumor-to-background fluorescence contrast ratio than the counterparts with positive charge. At 24 h post-injection, tumors and major organs were excised for *ex vivo* NIRF imaging to determine the tissue distribution of NPs. As shown in Fig. 10A, the biodistribution profiles of PEG^{5k}-CA_8 NPs were dramatically influenced by the surface charges of NPs. Although all the NPs demonstrated good tumor accumulation as a result of the EPR effect, the magnitude of tumor uptake for the neutral or negatively charged NPs was higher than positively charged NPs. The median fluorescence intensity (MFI) of tumors collected from mice injected with 6d-NP, 3d-NP, 1d-NP, Ac-NP, 1k-NP, 3k-NP and 6k-NP were 2326 ± 216, 2715 ± 356, 3182 ± 365, 2478 ± 163, 2208 ± 180, 2067 ± 246, and 1795 ± 209, respectively (Fig. 10B). In addition, compared to neutral NPs (Ac-NP), highly positive charged NPs (such as 3k-NP and 6k-NP) and highly negative charged NPs (6d-NP) had significantly higher NPs uptake in the liver ($P < 0.05$), while slightly negative charged NPs (1d-NP) had relatively lower liver uptake. Overall, PEG^{5k}-CA_8 NPs with highly positive surface charge exhibited the lowest tumor uptake but the highest liver uptake, whereas those with slightly negative charge exhibited the highest tumor uptake but the lowest uptake to all normal organs including liver and lung. The MFI ratios between tumor and liver for 6d-NP, 3d-NP, 1d-NP, Ac-NP, 1k-NP, 3k-NP and 6k-NP were 0.82, 1.28, 1.75, 1.18, 0.84, 0.60 and 0.40, respectively. Furthermore, the microscopic analysis of liver cryosections indicated that NPs were mainly taken up by the macrophages (Kupffer cells) in the liver, which were identified by the staining of F4/80 macrophage antigen marker (Fig. 10C). The uptake efficiency of NPs by the Kupffer cells in the liver increased as the surface charge density (especially positive charge) of the NPs increased, which was consistent with the results from the *in vitro* macrophage uptake studies.

4. Discussion

For the drug delivery application in cancer therapy, the nonspecific uptake of NPs by macrophages in the RES may be minimized through manipulation of particle size and surface charge [19,22]. For example, we have recently demonstrated that the biodistribution of PEG-oligocholic acid based micellar NPs depends greatly on the particle size [15]. The smaller PTX-loaded NPs (17–60 nm) preferentially accumulated in the tumor site, whereas most of the larger NPs (150 nm) were trapped by the liver and lung where many macrophages were located. Surface charge has also been reported to play a major role to regulate the NPs uptake by macrophages [10,12]. However, the results of these previous studies were confounded by other variable factors such as composition and particle size.

The conventional method to modulate the surface properties of NPs is usually through post-synthesis particle surface modification, which requires the addition of an excess amount of reactants to drive the chemical reaction, thus making it difficult to control the surface properties of NPs in a reproducible manner. The development of NPs by the self-assembling of pre-functionalized subunits would eliminate the need of post-particle modification, and may have less batch-to-batch variation [23]. In this study, PEG^{5k}-CA_8 telodendrimer (the micellar subunit) was functionalized by conjugating different number of anionic aspartic acids (negative charge) or cationic lysines (positive charge) to the distal end of PEG chain, followed by N-terminal acetylation. The aspartic acids or lysines derivatized PEG^{5k}-CA_8 amphiphilic copolymer self-assembled to form micelles in aqueous solution spontaneously. The surface charges of the resulting micellar NPs were determined by the number of aspartates or lysines linked to each subunit. The expected surface charge properties of these derivatized NPs were generally confirmed by the zeta potential measurement (Table 1) and electrophoretic properties in agarose gel (Figure 3). The acetylated NPs (Ac-NP) with an expected neutral charge were found to display slightly positive charge in water. This is probably due to the association of proton or metal ions with the PEG on the outer shell of micelles or the trace amount of remaining amines. Virtually, the surface charge modulation had negligible effects on the physical properties of PEG^{5k}-CA_8 NPs, such as morphology, size and stability. Therefore, this PEG^{5k}-CA_8 micellar nanoplatform is an excellent system for the study of the surface charge effect of NPs on their intracellular uptake by macrophages as well as their *in vivo* biodistribution in xenograft models.

Positively charged PEG^{5k}-CA_8 NPs were found to be more easily taken up by RAW 264.7 murine macrophages in serum-free medium compared to negatively charged and neutral NPs, and the tendency of NPs uptake increased accordingly with the increasing positive charge density, which was accordance with the previous results [2]. A possible explanation for this phenomenon could be the electrostatic interaction between the positive charge on the surface of NPs and the negative charge on the cell membrane (sialic acids and phospholipid head groups) of macrophages, which facilitate the internalization process of NPs. Interestingly, after pre-opsonization in fresh mouse serum, the uptake of positively charged NPs were slightly decreased, whereas the uptake of negatively charged NPs were considerably increased, especially for the highly negative charged NPs (6d-NP). This latter observation can be explained by the activation of membrane receptors on the cell surface by the NPs-bound serum protein, which triggers receptor-mediated endocytosis and promote cellular uptake of NPs. Unlike the negative charged NPs, the cellular uptake of positive charged NPs are generally very high, therefore, the formation of NPs-serum protein complex may actually interfere the electrostatic interactions between NPs and cell membrane, thus decrease the cell uptake of NPs. Our data also demonstrated that heat-inactivated mouse serum was less effective than fresh serum in promoting cellular uptake of negatively charged NPs by the macrophages. The known heat-labile opsonins in the serum which can interact specifically with certain membrane receptors are components in the complement system.

Thus, it suggests that complement system may be involved in the macrophage uptake process of different charged PEG^{5k}-CA_8 NPs. The role of the activation of the complement system in the uptake of NPs by macrophages has been previously reported [24].

Upon internalization, the majority of NPs with various surface charges were found to co-localize in the lysosomal compartment. Generally, NPs are first enclosed into early endosomes after uptake by the macrophages via endocytosis, and then early endosomes become mature and form late endosomes or multivesicular bodies, and eventually merge into lysosomes, which are acidic (approx. pH 4.8), and regarded as the principle hydrolytic compartment of the cell. Three different endocytosis inhibitors, including CPZ (clathrin-mediated endocytosis inhibitor), amiloride (macropinocytosis inhibitor) and filipin III (caveolae-mediated endocytosis inhibitor) were found to be able to inhibit the endocytosis of different charged PEG^{5k}-CA_8 NPs. The relative potency of these endocytosis inhibitors was as follows: CPZ > amiloride > filipin III. As immunoglobulins (Igs) are known substrates for clathrin-mediated endocytosis, those NPs opsonized by Igs in the fresh mouse serum are more likely taken up by macrophages through this pathway. However, in the serum-free medium where Igs are absent, different charged NPs could also be internalized into macrophages to varying extent. This suggests that some other nonspecific pathways, such as macropinocytosis, may be also involved in the endocytic process of NPs.

The study of the compatibility of NPs with blood cells, also called hematocompatibility, is extremely important especially when NPs are used in the injectable drug formulations. The intravenously injected NPs will first encounter a large fraction of blood cells in the blood prior to distribution into tissues, and hemolysis is one of its potential hematotoxicities. The influence of surface charge on the hemolytic activity of blank NPs was examined in the present study. Negatively charged NPs were not hemolytic, whereas positively charged NPs were associated with erythrocyte damage in a dose-dependent manner, and the hemolytic tendency increased in proportion to the positive charge density of NPs. This finding was also supported by some previous investigations. For example, the unprotected primary amines (positive charge) on the surface of polyamidoamine (PAMAM) [25], polypropylene imine (PPI) [26], and polylysine (PLL) [27] dendrimers have been shown to induce hemolytic activity. However, blockade of these primary amines resulted in a dramatic decrease in hemolysis. The hemolysis induced by positively charged NPs may be caused by the strong electrostatic interaction between the particles and erythrocyte membrane, which facilitates the insertion of the whole particles or dissociated amphiphilic monomeric units into the membrane, and results in disruption of erythrocyte cell membrane. It is, however, important to note that the hemolytic activities of these micellar NPs decreased significantly when hydrophobic drugs such as PTX were loaded (unpublished data). This can easily be explained by the increase in hydrophobic interactions at the micellar core when PTX is present, thus preventing dissociation of the amphiphilic monomeric units from the micellar NPs.

In the *in vivo* biodistribution study, the high tumor uptake exhibited by the slightly negatively charged NPs (1d-NP) might be due to their prolonged blood circulation time. On the contrary, rapid clearance of the highly charged NPs by RES resulted in relatively short half-life and low tumor uptake. As the NPs are mainly eliminated by the phagocytic uptake in RES and liver is the main organ in RES, the extent of sequestration of NPs by liver has been reported to correlate with the level of blood retention [28]. Our data in this study demonstrated that highly positive or negative charge significantly increased the liver uptake of PEG^{5k}-CA_8 NPs; whereas slightly negative charge considerably decreased their liver uptake, protecting the NPs from phagocytosis. The uptake profiles of PEG^{5k}-CA_8 NPs with various surface charges by the Kupffer cells in the liver are consistent with the results from the *in vitro* macrophage uptake studies, as well as some previous reports concerning the

effect of surface charge on the macrophage uptake of inorganic NPs [9], dendrimers [29], albumin NPs [30], and polymeric NPs [11]. The absorption of plasma proteins (opsonins) on the nanoparticle surface is regarded as a key factor in the process of phagocytic recognition. There is some evidence that highly charged NPs have a much higher opsonization rate than neutral or slightly charged NPs of the same size [19]. Therefore, the relative low uptake of slightly negatively charged NPs in the liver may be attributed to the low opsonization rate as well as electrostatic repulsion that minimize the recognition and non-specific uptake by macrophages in the liver.

As demonstrated in the present study, physicochemical characteristics of NPs (particle size and surface charge) had tremendous impacts on their pharmacokinetic and pharmacodynamic profiles such as biodistribution, elimination and tumor targeting property. Therefore, a well designed drug delivery system should possess with optimal particle size and suitable surface charge density that promise efficient drug delivery to the target site. The tumor targeting property of NPs may also be influenced by the variation of tumor characteristics such as tumor type and tumor size [31]. Furthermore, by incorporating some of the targeting ligands, the utility of NPs as a therapeutic agent or carrier can be broadened. Preliminary data from our recent studies suggest that NPs when decorating with high-affinity and high-specificity tumor targeting ligands exhibit preferential tumor accumulation and superior therapeutic efficacy both *in vitro* and *in vivo*.

5. Conclusions

PEG^{5k}-CA_8 NPs with high surface charge, either positive or negative, tend to be taken up nonspecifically by macrophages *in vitro* and *in vivo*, resulting in high uptake of NPs in the liver after systematic administration. In contrast, PEG^{5k}-CA_8 NPs with slightly negative charge (one aspartic acid per telodendrimer) demonstrated preferential uptake at the tumor site but not normal organs including liver. We believe that the optimal surface charge of NPs designed for use as drug delivery carrier in cancer therapy should be slightly negative. This will minimize the undesirable rapid elimination of NPs from the blood circulation, and facilitate their accumulation at the tumor sites.

Supplementary Material

Refer to Web version on PubMed Central for supplementary material.

Acknowledgments

The authors thank the financial support from NIH/NCI R01CA115483, R01CA140449 and US Department of Defense Breast Cancer Research Program Postdoctoral Training Award (W81XWH-10-1-0817).

References

[1]. Matsumura Y, Maeda H. A new concept for macromolecular therapeutics in cancer chemotherapy: mechanism of tumoritropic accumulation of proteins and the antitumor agent smancs. Cancer Res 1986;46(12 Pt 1):6387–92. [PubMed: 2946403]

[2]. Alexis F, Pridgen E, Molnar LK, Farokhzad OC. Factors affecting the clearance and biodistribution of polymeric nanoparticles. Mol Pharm 2008;5(4):505–15. [PubMed: 18672949]

[3]. Davis ME, Chen ZG, Shin DM. Nanoparticle therapeutics: an emerging treatment modality for cancer. Nat Rev Drug Discov 2008;7(9):771–82. [PubMed: 18758474]

[4]. Gref R, Minamitake Y, Peracchia MT, Trubetskoy V, Torchilin V, Langer R. Biodegradable long-circulating polymeric nanospheres. Science 1994;263(5153):1600–3. [PubMed: 8128245]

[5]. Zahr AS, Davis CA, Pishko MV. Macrophage uptake of core-shell nanoparticles surface modified with poly(ethylene glycol). Langmuir 2006;22(19):8178–85. [PubMed: 16952259]

[6]. Schipper ML, Iyer G, Koh AL, Cheng Z, Ebenstein Y, Aharoni A, et al. Particle size, surface coating, and PEGylation influence the biodistribution of quantum dots in living mice. Small 2009;5(1):126–34. [PubMed: 19051182]

[7]. Thorek DL, Tsourkas A. Size, charge and concentration dependent uptake of iron oxide particles by non-phagocytic cells. Biomaterials 2008;29(26):3583–90. [PubMed: 18533252]

[8]. Daniel MC, Tsvetkova IB, Quinkert ZT, Murali A, De M, Rotello VM, et al. Role of surface charge density in nanoparticle-templated assembly of bromovirus protein cages. ACS Nano 2010;4(7):3853–60. [PubMed: 20575505]

[9]. Osaka T, Nakanishi T, Shanmugam S, Takahama S, Zhang H. Effect of surface charge of magnetite nanoparticles on their internalization into breast cancer and umbilical vein endothelial cells. Colloids Surf B Biointerfaces 2009;71(2):325–30. [PubMed: 19361963]

[10]. Juliano RL, Stamp D. The effect of particle size and charge on the clearance rates of liposomes and liposome encapsulated drugs. Biochem Biophys Res Commun 1975;63(3):651–8. [PubMed: 1131256]

[11]. He C, Hu Y, Yin L, Tang C, Yin C. Effects of particle size and surface charge on cellular uptake and biodistribution of polymeric nanoparticles. Biomaterials 2010;31(13):3657–66. [PubMed: 20138662]

[12]. Chung TH, Wu SH, Yao M, Lu CW, Lin YS, Hung Y, et al. The effect of surface charge on the uptake and biological function of mesoporous silica nanoparticles in 3T3-L1 cells and human mesenchymal stem cells. Biomaterials 2007;28(19):2959–66. [PubMed: 17397919]

[13]. Yamamoto Y, Nagasaki Y, Kato Y, Sugiyama Y, Kataoka K. Long-circulating poly(ethylene glycol)-poly(D,L-lactide) block copolymer micelles with modulated surface charge. J Control Release 2001;77(1–2):27–38. [PubMed: 11689257]

[14]. Xiao K, Luo J, Fowler WL, Li Y, Lee JS, Xing L, et al. A self-assembling nanoparticle for paclitaxel delivery in ovarian cancer. Biomaterials 2009;30(30):6006–16. [PubMed: 19660809]

[15]. Luo J, Xiao K, Li Y, Lee JS, Shi L, Tan YH, et al. Well-defined, size-tunable, multifunctional micelles for efficient paclitaxel delivery for cancer treatment. Bioconjug Chem 2010;21(7):1216–24. [PubMed: 20536174]

[16]. Li Y, Xiao K, Luo J, Lee J, Pan S, Lam KS. A novel size-tunable nanocarrier system for targeted anticancer drug delivery. J Control Release 2010;144(3):314–23. [PubMed: 20211210]

[17]. Liu J, Lee H, Allen C. Formulation of drugs in block copolymer micelles: drug loading and release. Curr Pharm Des 2006;12(36):4685–701. [PubMed: 17168772]

[18]. Mosmann T. Rapid colorimetric assay for cellular growth and survival: application to proliferation and cytotoxicity assays. J Immunol Methods 1983;65(1–2):55–63. [PubMed: 6606682]

[19]. Dobrovolskaia MA, Aggarwal P, Hall JB, McNeil SE. Preclinical studies to understand nanoparticle interaction with the immune system and its potential effects on nanoparticle biodistribution. Mol Pharm 2008;5(4):487–95. [PubMed: 18510338]

[20]. Nam HY, Kwon SM, Chung H, Lee SY, Kwon SH, Jeon H, et al. Cellular uptake mechanism and intracellular fate of hydrophobically modified glycol chitosan nanoparticles. J Control Release 2009;135(3):259–67. [PubMed: 19331853]

[21]. Peng L, Liu R, Marik J, Wang X, Takada Y, Lam KS. Combinatorial chemistry identifies high-affinity peptidomimetics against alpha4beta1 integrin for in vivo tumor imaging. Nat Chem Biol 2006;2(7):381–9. [PubMed: 16767086]

[22]. Balogh L, Nigavekar SS, Nair BM, Lesniak W, Zhang C, Sung LY, et al. Significant effect of size on the in vivo biodistribution of gold composite nanodevices in mouse tumor models. Nanomedicine 2007;3(4):281–96. [PubMed: 17962085]

[23]. Gu F, Zhang L, Teply BA, Mann N, Wang A, Radovic-Moreno AF, et al. Precise engineering of targeted nanoparticles by using self-assembled biointegrated block copolymers. Proc Natl Acad Sci U S A 2008;105(7):2586–91. [PubMed: 18272481]

[24]. Gaucher G, Asahina K, Wang J, Leroux JC. Effect of poly(N-vinyl-pyrrolidone)-block-poly(D,L-lactide) as coating agent on the opsonization, phagocytosis, and pharmacokinetics of biodegradable nanoparticles. Biomacromolecules 2009;10(2):408–16. [PubMed: 19133718]

[25]. Domanski DM, Klajnert B, Bryszewska M. Influence of PAMAM dendrimers on human red blood cells. Bioelectrochemistry 2004;63(1–2):189–91. [PubMed: 15110271]

[26]. Agashe HB, Dutta T, Garg M, Jain NK. Investigations on the toxicological profile of functionalized fifth-generation poly (propylene imine) dendrimer. J Pharm Pharmacol 2006;58(11):1491–8. [PubMed: 17132212]

[27]. Shah DS, Sakthivel T, Toth I, Florence AT, Wilderspin AF. DNA transfection and transfected cell viability using amphipathic asymmetric dendrimers. Int J Pharm 2000;208(1–2):41–8. [PubMed: 11064210]

[28]. Sheng Y, Liu C, Yuan Y, Tao X, Yang F, Shan X, et al. Long-circulating polymeric nanoparticles bearing a combinatorial coating of PEG and water-soluble chitosan. Biomaterials 2009;30(12):2340–8. [PubMed: 19150737]

[29]. Perumal OP, Inapagolla R, Kannan S, Kannan RM. The effect of surface functionality on cellular trafficking of dendrimers. Biomaterials 2008;29(24–25):3469–76. [PubMed: 18501424]

[30]. Roser M, Fischer D, Kissel T. Surface-modified biodegradable albumin nano- and microspheres. II: effect of surface charges on in vitro phagocytosis and biodistribution in rats. Eur J Pharm Biopharm 1998;46(3):255–63. [PubMed: 9885296]

[31]. Xiao K, Luo J, Li Y, Xiao W, Lee J, Gonik AM, et al. The passive targeting of polymeric micelles in various types and sizes of tumor models. Nanosci Nanotechnol Lett 2010;2(2):79–85.

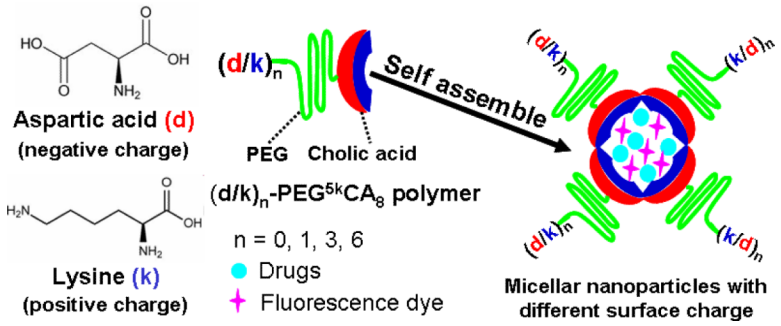

Fig.1.

Schematic representation of the design of PEG^{5k}-CA_8 micellar NPs with various surface charges. Different number (n = 0, 1, 3 and 6) of D-aspartic acids (d) or D-lysines (k), which have anionic or cationic characters at physiological pH (7.4), respectively, were conjugated onto the distal end of PEG strands constituting a shell layer of the PEG^{5k}-CA_8 micellar NPs to modulate the surface charge. The N-terminal amino group was acetylated.

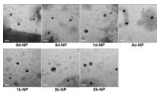

Fig.2.
The morphology and particle size of different charged PEG^{5k}-CA_8 NPs measured by transmission electron microscopy (TEM).

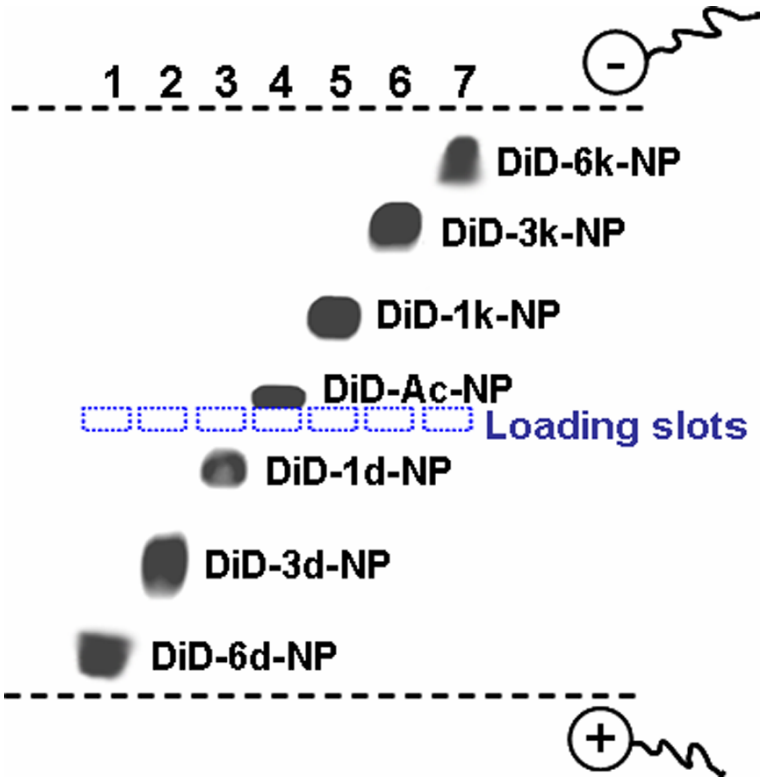

Fig.3.

Electrophoresis of DiD labeled PEG^{5k}-CA_8 NPs with various surface charge densities in 1% agarose gel. The DiD signals in the NPs were imaged using Kodak imaging station with excitation at 625 nm and emission at 700 nm.

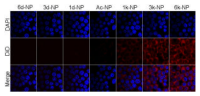

Fig.4.

Confocal fluorescent microscopy showing cellular uptake of NPs in RAW 264.7 murine macrophages after 2 hours of incubation with DiD-labeled PEG^{5k}-CA_8 NPs with various surface charges in serum-free medium.

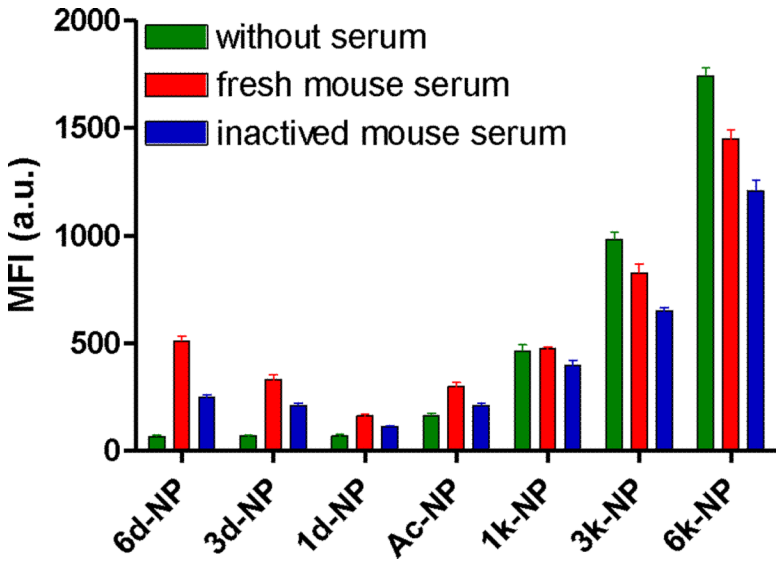

Fig.5.

The effect of the pre-opsonization of NPs in fresh or inactive mouse serum on their cellular uptake in RAW 264.7 murine macrophages. Data represent mean ± SEM (n = 3).

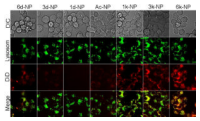

Fig.6.

Intracellular tracking of different charged PEG^{5k}-CA_8 NPs in RAW 264.7 macrophages. RAW 264.7 macrophages were incubated with DiD (red) labeled PEG^{5k}-CA_8 NPs with various surface charges for 2 hours in medium with 10% fresh mouse serum, after which the cells were labeled with lysosome tracker (green) for 30 min before imaging by confocal microscopy. Co-localization of NPs with lysosome appears yellow in merged images, indicating that the NPs are present in the lysosome.

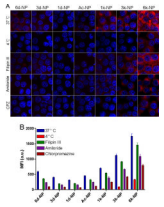

Fig.7.

The cellular uptake pathways of different charged PEG^{5k}-CA$_8$ NPs in macrophages. RAW 264.7 cells were either pre-incubated at 4 °C for 3 h, followed by incubation with DiD-labeled PEG^{5k}-CA$_8$ NPs with various surface charges at 4 °C for 2 h; or pre-treated with different endocytosis inhibitors such as filipin III (1 μg/mL), amiloride (50 μM) and chlorpromazine (CPZ, 10 μg/mL) at 37 °C for 1 h, followed by incubation with different charged PEG^{5k}-CA$_8$ NPs at 37 °C for 2 h. (A) Confocal microscopy images of cellular uptake. Nuclei were stained by DAPI (blue). (B) Quantitative analysis of the cellular uptake by flow cytometry. Data represent mean ± SEM (n = 3).

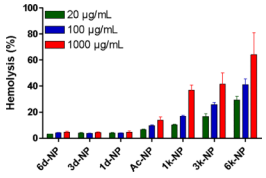

Fig.8.

In vitro red blood cells (RBCs) lysis. Different charged PEG^{5k}-CA_8 NPs were incubated with human erythrocyte suspension for 4 h at 37 °C. RBCs lysis was determined spectrophotometrically (λ = 540 nm) based on hemoglobin level. PBS was used as negative control, and Triton-100 was used as positive control. Data represent mean ± SEM (n = 3).

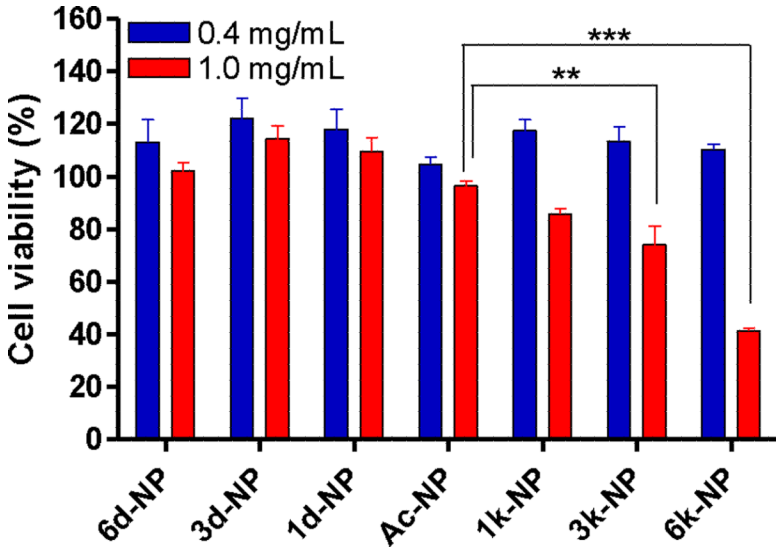

Fig.9.

The effect of surface charge on the cell viability of PEG^{5k}-CA_8 NPs against RAW 264.7 cells measured by MTT assay. Data represent mean ± SEM (n = 3). *: $p < 0.05$, **: $p < 0.01$, ***: $p < 0.001$.

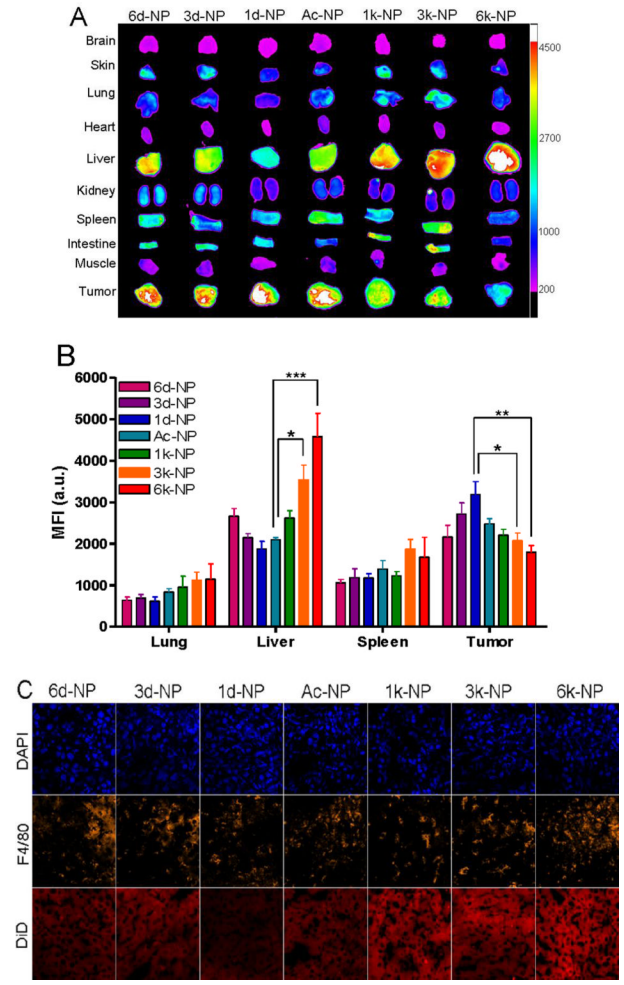

Fig.10.

Biodistribution of different charged PEG^{5k}-CA$_8$ NPs after intravenous injection in SKOV-3 tumor bearing mice. (A) Representative *ex vivo* near-infrared (NIRF) optical images of tumor and major organs excised at 24 h after intravenous injection of DiD loaded PEG^{5k}-CA$_8$ NPs with various surface charges. (B) Quantitative fluorescence intensities of tumors and organs from *ex vivo* images (n = 3). (C) Microscopic images of liver cryo-section. The nuclei were stained by DAPI (blue), and macrophages were stained by F4/80 antibody (yellow), and the signals of DiD (red) were acquired using Olympus FV1000 laser scanning confocal microscopy. *: $p < 0.05$, **: $p < 0.01$, ***: $p < 0.001$.

Table 1

The physicochemical characteristics of different charged PEG^{5k}-CA_8 NPs

Telodendrimers	Particle size (nm)	Particle size after DiD/PTX loading (nm)*	Zeta potential (mV)
6d-$PEG^{5k}CA_8$	21 ± 4	24 ± 7	−26.9 ±1.7
3d-$PEG^{5k}CA_8$	17 ± 3	24 ± 4	−17.5 ± 0.9
1d-$PEG^{5k}CA_8$	18 ± 4	26 ± 5	−8.5 ± 1.8
Ac-$PEG^{5k}CA_8$	18 ± 3	27 ± 6	3.6 ± 0.8
1k-$PEG^{5k}CA_8$	19 ± 3	25 ± 5	18.5 ± 3.1
3k-$PEG^{5k}CA_8$	17 ± 4	23 ± 7	29.5 ± 1.2
6k-$PEG^{5k}CA_8$	19 ± 4	25 ± 6	37.0 ± 2.9

*2% DiD fluorescence dye along with paclitaxel drug (1 mg/mL) were encapsulated into the core of different charged PEG^{5k}-CA_8 NPs to track the cellular uptake and *in vivo* biodistribution of NPs.